CHAPTER 3

Mustard seeds derived fluorescent carbon quantum dots and their peroxidase-like activity for colorimetric detection of H_2O_2 and ascorbic acid in a real sample

3.1. Introduction

In recent years, carbon quantum dots (CQDs) have attracted much attention in scientific community due to its ease of synthetic methodology and tremendous applications in various field of applications including catalysis, biosensors, medicines, food industry, corrosion protection, LED's devices, medical diagnostics, wastewater treatment, and agrochemical production [H. Jia *et al.* (2016), Y. Lin *et al.* (2014), P.K. Khanna *et al.* (2007), V. Arul *et al.* (2017), D. Jampaiah *et al.* (2016), R. Wolfenden *et al.* (2001), N. Vasileva *et al.* (2009), B. Wang *et al*. (2018)]. The small size and high surface area of CQDs impart the enormous catalytic efficiency and vigorous substrate specificity. Peroxidase is a natural enzyme which catalyzes the decomposition of peroxide and prevents the biological cell from the toxic materials [X. Chen *et al.* (2014)]. However, the natural enzymes have many disadvantages such as high rate of denaturation in harsh condition and costly purification and preservation processes [Y. Chen *et al.* (2013), M. Hosseini *et al.* (2017)]. Therefore, to subside the problem of the natural enzyme, there is an urgent need to develop an artificial enzyme to showed peroxidase-like mimic-activity like natural enzyme Horseradish peroxidase (HRP). Moreover, the artificial enzymes have several advantageous properties such as low cost, high stability, non-toxic, eco-friendly, commercially available, ease preparation and purifications cost [H. Wei *et al.* (2013)]. Previously, many of the research group have been reported the variety of materials to showed the peroxidase-like mimic activity such as iron oxide-based nanomaterial [F. Yu *et al.* (2009)], cerium-based nanomaterial [A. Asati *et al.* (2009), T. Pirmohamed *et al.* (2010)], transition metal dichalcogenides [D. Kong *et al.* (2013), Q. Lu *et al.* (2016)], metal organic frameworks [W. Dong *et al.* (2017)]. Additionally, Deshetti Jampaiah *et al.* and Wei Chen *et al.* has been

reported CeO_2 Nanorods and cupric oxide nanoparticle which exhibited the peroxidase-like activity [Y. Chai *et al.* (2018)]. However, these nanomaterials are synthesized by toxic chemicals, metal ions and costly reagents which showed the detrimental effect on human health and the environment [H. Wei *et al*. (2008), T. Pal *et al*. (2018)].

In addition, the carbon-based nanomaterial such as graphene oxide [H.H *et al.* (2017)], carbon nanotubes [Y. Song *et al.* (2010)], carbon nanodots [W. Shi *et al*. (2011)], and carbon nitride sheets [T. Lin *et al.* (2014)], and graphene quantum dots [X. Wu *et al.* (2014)], possessed peroxidase-like or superoxide dismutase [W. Wang *et al*. (2012)], like activity. They have low cytotoxicity, excellent biocompatibility, high surface area, high substrate specificity, high photo-stability and unique excitation dependent fluorescence properties [M. Shamsipur *et al*. (2018), N. Amin *et al*. (2018)].

Herein, we have demonstrated the one-step hydrothermal synthesis of fluorescent carbon quantum dots from the seeds of mustards (M-CQDs) (Scheme1). The current reported method was found to be completely green, rapid, facile, and of lower cost as compared to other methods [H. Peng *et al.* (2017), R. Purbia *et al.* (2018)]. The synthesized M-CQDs was thoroughly characterized by a various instrumental method such as TEM, FT-IR, P-XRD, XPS analysis, UV-Visible absorption spectroscopy, and fluorescence spectroscopy. M-CQDs possessed peroxidase-like catalytic activity and catalyzed the oxidation of chromogenic subtract TMB in the presence of H_2O_2. The H_2O_2 dependent catalytic activities of M-CQDs act as a colorimetric sensor for the detection of natural reductant ascorbic acid (AA) in common fresh fruits [B. Yang *et al.* (2016)]. Alternatively, the determination of AA is performed using different techniques such as chromatographic [P. Jiang *et al.* (2017)],

electrochemical [M.M *et al.* (2018)] and spectroscopic techniques [J. Wang *et al.* (2018)]. However, these analytical techniques have several drawbacks in the form of huge time consumption in sample preparation, use of hazardous chemicals and reagents, sophisticated and costly instrumentations [Q. Nie *et al.* (2018), D. Ji *et al.* (2018)].

3.2. Materials and method

3.2.1. Hydrothermal Synthesis M-CQDs

Firstly, 2.0 g of mustard seeds were crushed in a mortar pestle and dissolved in 50 mL of ultrapure water to make the suspension. Afterward, the suspension was poured in Teflon-line autoclave and kept at 180 °C for 4 hrs **(Scheme 3.1)**. After completion of the reaction, the autoclave was cooled naturally at room temperature, and the obtained solution was centrifuged at 15000 rpm for 20 minutes to remove the foreign and agglomerated particles. Finally, the prepared M-CQDs solution was collected and kept at 4 °C for characterizations and application.

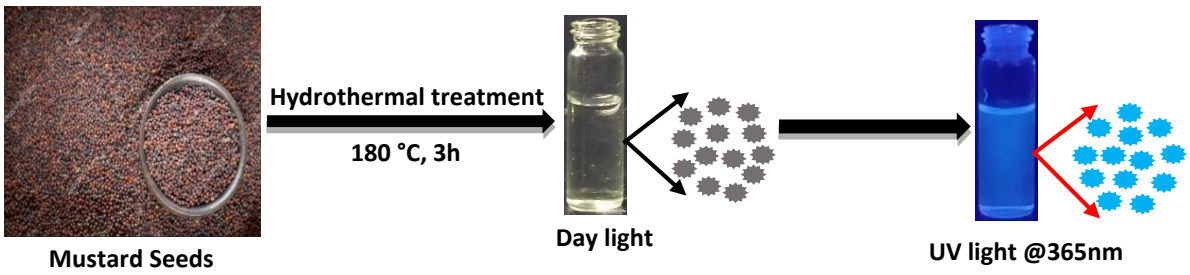

Scheme 3.1 Illustration of the hydrothermal synthesis of carbon quantum dots by mustard seeds.

3.2.2. Quantum yield determination

Fluorescence quantum yield of M-CQDs was determined with reference to quinine sulphate (QY = 54% at 340 nm excitation). The absorbance (below 0.1) and the integrated intensity of the quinine sulphate solution in 0.1 M H_2SO_4 were determined, the same

parameter were obtained for M-CQDs at the same excitation wavelength, and quantum yields were calculated from Table 3.

Table 3. Fluorescence quantum yield determination of M-CQDs with reference to quinine sulphate at excitation wavelength 340 nm from the equation (2.1).

Sample	Integrated intensity at 340 nm	Absorbance at 340 nm	Quantum Yield (%)
Quinine Sulphate (Reference)	42672.467	0.047	54
M-CQDs	3123.360	0.040	4.6

3.2.3. Investigation of Peroxidase- like mimetic activity

The peroxidase-like mimetic activity of M-CQDs was planned in the oxidation of TMB as a chromogenic substrate in the presence of H_2O_2. For this, 50 µL of M-CQDs was added into the reaction system containing 50 µL TMB, (1.0 mM) 50 µL H_2O_2 (1.0 mM) 1.0 mL of 0.2 M sodium acetate (NaAc) buffer at pH 4. It was observed that the color of the incubated samples showed the instant change in color from transparent to intense blue and intense spectra at 652 nm. However, the reaction system devoid of M-CQDs (TMB+H_2O_2 and TMB+M-CQDs) did not show any change in color as well as the development of UV spectra.

3.2.4. Analysis of hydroxyl radical

The decomposition of H_2O_2 involves the generation of hydroxyl radical ($^{\bullet}OH$) which oxidizes TMB in the presence of M-CQDs which was considered as a base for $^{\bullet}OH$ radical scavenging test. In the current study, methyl alcohol and isopropyl alcohol were used as an $^{\bullet}OH$ scavenger which was added into the optimum reaction condition, and the change in UV-visible spectra was recorded.

3.2.5. Detection of H_2O_2 by colorimetric method

In the typical reaction, 50 μL of TMB (9 mM), 50 μL M-CQDs and 0.2 mM NaAc buffer at pH 4 were treated with the different concentration of H_2O_2 (0.2 to 4.0 mM) and the absorbance spectra were recorded after 15 minutes via the spectrophotometer. The LOD was calculated to be 0.015 mM by the linear calibration plot using formula $3\sigma/m$ with S/N=3.

3.2.6. Detection of Ascorbic Acid (AA)

The colorimetric detection of AA was investigated using M-CQDs under the optimum condition where 50 µL of 9 mM TMB + 50 µL of 9 mM H_2O_2 + 50 µL M-CQDs were mixed into 0.2M NaAc buffer at pH 4 which produced blue color. When the different concentration of AA (0 to 70 µM was added into the blue color oxidized TMB solution, it was noticed that on increasing the AA concentration, the blue color gradually changed to colorless and UV- visible spectra recorded at 652 nm, showed a subsequent decrease the absorbance intensity. The interference of other reducing agent were performed as similar way by replacing the AA with different reducing agent.

3.2.7. Colorimetric detection of AA in real fruit juices

The fresh fruits were brought from the market and washed, air dried and weighed 25 gm of the edible part containing AA. Furthermore, the removes of impurities from fruits juice dissolve in 3 mL ultrapure water through the centrifuge at 4500 rpm for 25 minutes at 5^0C. After that, the extract fruit juice filtered accurately and added 50 μl different real sample into ox-TMB solution with recorded UV-visible absorption spectra. Finally, the absorbance decreases with the addition of more containing AA real fruit juices respectively.

3.2.8. Experimental methodology

The synthesized fluorescent M-CQDs were characterized by different spectroscopic techniques such as Transmission Electron Microscopy (TEM), Powdered X-Ray Diffraction (P-XRD), Fourier Transformed Infrared Spectroscopy (FT-IR), and X-ray photoelectron spectroscopy (XPS). UV-visible absorbance spectra were obtained using a Thermo Scientific, Evolution 201 spectrophotometer. Size and shape were measured *via* TEM, TECHNAI G^2 20 S-TWIN. XRD spectra were obtained using Rigaku MiniFlex 600 with a Cu Kα radiation source and Ni filter at the scanning rate of $3°min^{-1}$. The functional groups of organic/inorganic compounds were identified by FTIR, Perkin Elmer Spectrum 100. Chemical compositions were identified by XPS, AMICUS.

3.3. Results and discussion

3.3.1. Characterizations

The exact shape and size of M-CQDs were identified by the TEM analysis which is based on the interaction or transfer of electrons through M-CQDs to form an image. The typical TEM image is shown in **(Figure 3.1a)** which revealed the presence of mono-dispersed, spherical M-CQDs. Inset of **Figure 3.1a** presents the typical SAED micrograph, the broad circular rings indicated the amorphous nature of the prepared M-CQDs**.** The size of M-CQDs has distributed in the narrow range 2 to 8 nm with an average size of 4.58 ± 0.26 nm which was calculated by counting 150 particles **(Figure 3.1b)**. The P-XRD diffraction pattern illustrated a broad peak at $2\theta = 23.4^o$ which corresponded to (002) plane of M-CQDs as shown in **Figure 3.1c** [D. Bano *et al.* (2018)]. These results indicated that the synthesized M-CQDs were amorphous and graphitic in nature. To illustrate the different functional groups of M-CQDs, FT-IR analysis was performed on KBr pellets which showed the presence of characteristic peaks at 3438 cm^{-1}(ν_s = OH/NH), 2923 cm^{-1}(ν_s = sp^2 -CH),

2852cm^{-1}(ν_s = sp^3 –CH), 1622 cm^{-1} (ν_s = C=O), 1275 cm-^{1}(ν_s = -C=C) and 1023 cm^{-1}(ν_s = C-O-C) as shown in **(Figure 3.1d)** [A. Zhu *et al.* (2012), J. Yu *et al*. (2016)] This result indicated that the M-CQDs was functionalized with –OH, -NH and C=O functional group. The zeta potential of M-CQDs was found to be -4.7 mV, indicated the presence of negatively charge functional group on the surface which enhanced the hydrophilicity and solubility of M-CQDs in aqueous solution **(Figure 3.2).**

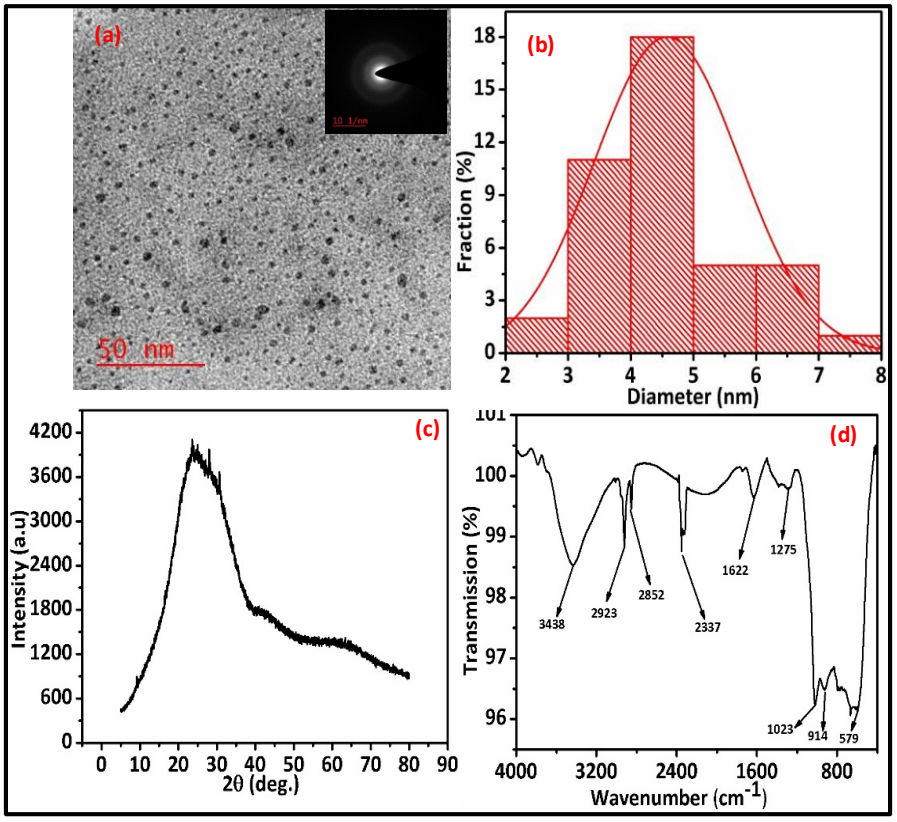

Figure 3.1 (a) TEM micrograph and SAED (inset) of M-CQDs (b) Size distribution (c) P-XRD pattern and (d) FT-IR spectra of as-synthesized M-CQDs.

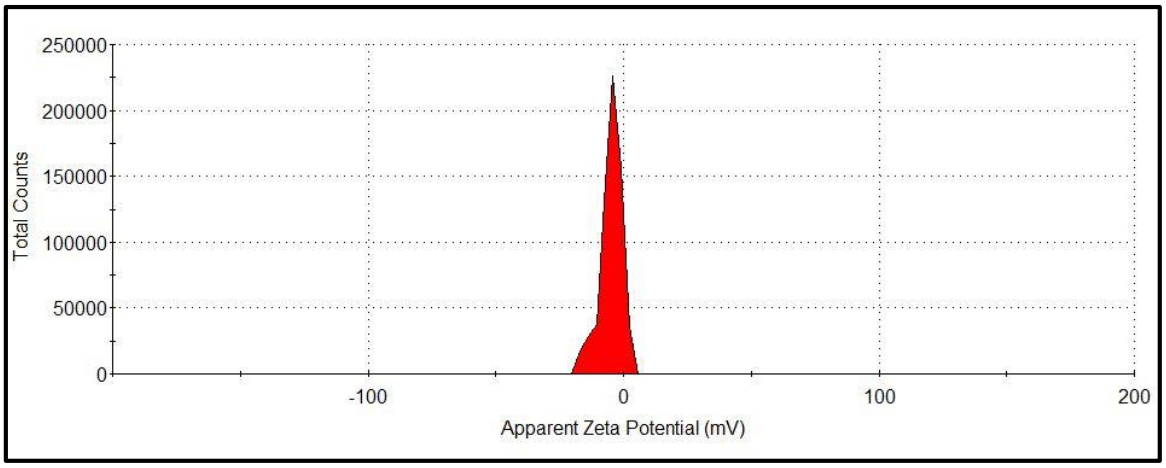

Figure 3.2 Zeta potential profile of as-synthesized M-CQDs

The XPS measurements were performed to determine the elemental composition and surface functional state of M-CQDs as shown in **(Figure 3.3.)**. The wide range XPS spectrum showed the characteristic peaks at 285.19 eV, 400 eV, and 530 eV, which confirmed that M-CQDs was mainly composed of C, N, and O **(Figure 3.3a)**. The C1s spectra showed four peaks at 285.19 eV, 286.10 eV, 287.16 eV, and 288.44 eV which suggested the presence of C-C, C=C, C-N/C-O, and C=O bonds respectively as shown in **Figure 3.3b** [J. Yu *et al*. (2016)]. The N 1s spectrum indicated the presence of three peaks at 400.24 eV, 401.00 eV, and 401.71 eV which corresponded to the presence of N-H, C-N-C, and N-H bonds respectively **(Figure 3.3c).** The XPS spectrum of O 1s **(Figure 3.3d)** showed the presence of four peaks at 532.93 eV, 533.65 eV, 534.30 eV, 534.97 eV, which were due to the presence of C=O, C-O-C, C-OH, and COO^- respectively. The XPS and FT-IR analysis were in good agreement with each other and confirmed the successful synthesis of M-CQDs.

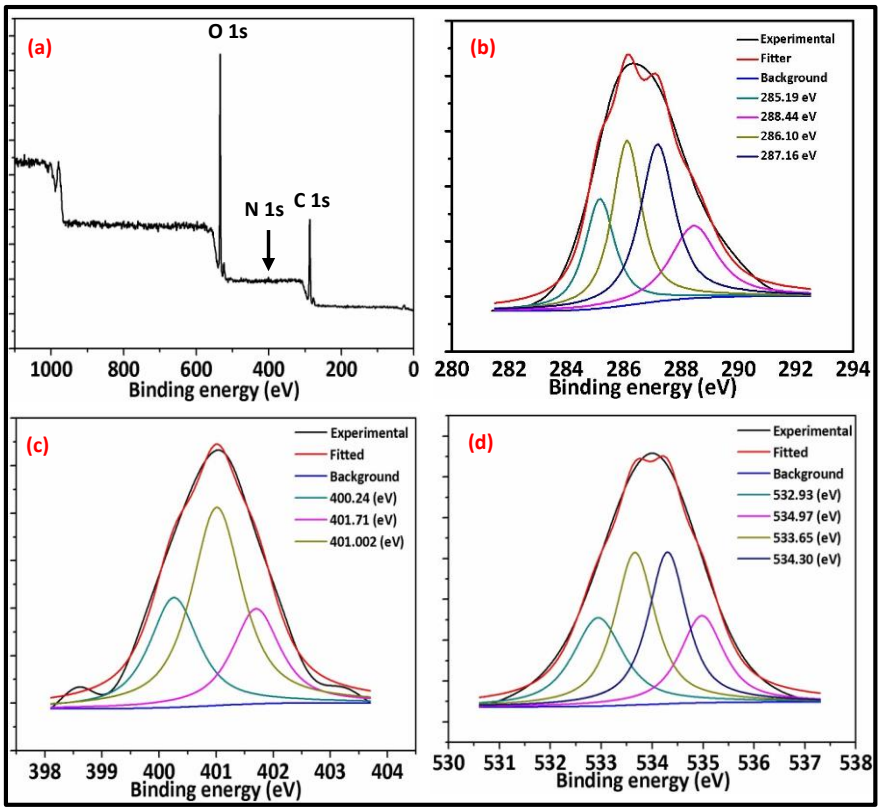

Figure 3.3 (a) XPS survey spectrum (b) C1s (c) N 1s and (d) O 1s spectra of as-synthesized M-CQDs.

3.3.2. Photophysical properties

To investigate the photophysical behavior of as-synthesized M-CQDs, UV- visible absorption and fluorescence spectra were recorded as shown in **Figure 3.4.** UV-visible spectrum of the aqueous solution of M-CQDs showed the two peaks at 245 nm, and 312 nm, the peak at 245 nm ascribed to π-π* transition whereas the peak at 312 nm was due to n-π* transition **(Figure 3.4a)** [Y. Zhang *et al.* (2015)]. Moreover, the fluorescence spectrum of M-CQDs exhibited excitation-dependent emission behavior. When M-CQDs was excited at 270 nm showed emission intensity at 430 nm, as the excitation wavelength increase (270 to 320 nm) emission intensity increase with a hypsochromic shift of 26 nm. Furthermore, increasing

the excitation wavelength maximum emission occurred at 423 nm at the excitation wavelength 330 nm **(Figure 3.4b)**.

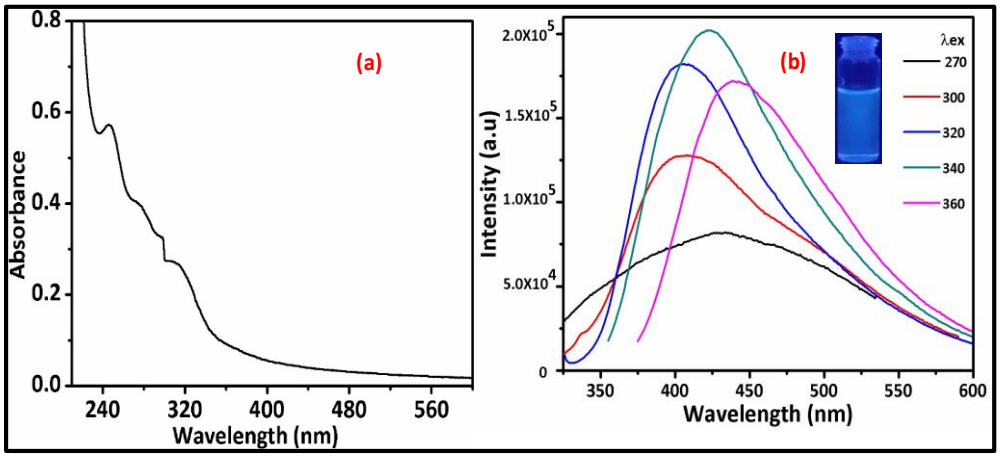

Figure 3.4 (a) UV-visible absorption spectrum and (b) Excitation dependent emission spectrum of synthesized M-CQDs.

The excitation-dependent emission behavior arose due to the surface defect of M-CQDs by the presence of different functional moieties [Y. Hu *et al.* (2017)]. The aqueous solution of M-CQDs showed blue color fluorescence under UV-light at 365 nm **(inset Figure 3.4b)**. Additionally, the fluorescence quantum yield of M-CQDs was 4.6 % which is appreciable for various application such as sensing, bio-imagine etc. The stability of M-CQDs was investigated at different pH, salt concentration and exposure time. From the **(Figure 3.5)** UV- visible absorption spectra of M-CQDs at different pH, it could be emphasized that in acidic medium (pH = 2 to 6), there was little effect on their absorption properties but in basic and neutral medium (7 to 12) absorption was highly affected. The effect of pH in the basic medium was due deprotonation of functional moieties of M-CQDs which leads to change in molecular state [Y. Song *et al.* (2014)].

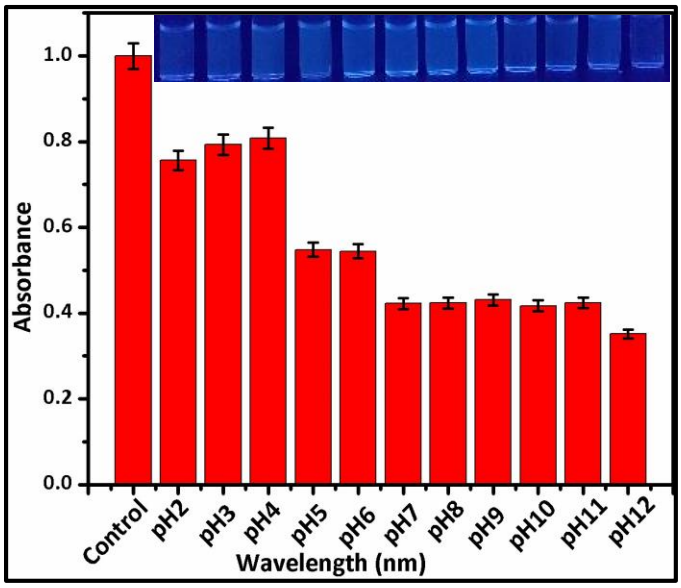

Figure 3.5 Absorbance of M-CQDs at different pH with corresponding photograph under UV- light (λ_{ex}= 365 nm**).**

This was further proved by the photograph taken under UV-light **(inset Figure 3.5).** Addition to this, the stability and effect of salt stress on M-CQDs was investigated by treated the M-CQDs with different concentration of KCl solution. From the **(Figure 3.6a)** showed there was negligible change in absorption spectra and no fluorescence quenching **(inset Figure 3.6a)** was observed under UV-light even in high KCl solution, this result confirmed that the functional group of M-CQDs was resisted to the high salt concentration which is a desirable property for broad-scale application of CQDs**.**

Furthermore, the photostability of M-CQDs was investigated by exposure of normal light for 8 h, and there was no obvious change in their absorption properties ensured the high photostability and long durability of synthesized M-CQDs **(Figure 3.6b).**

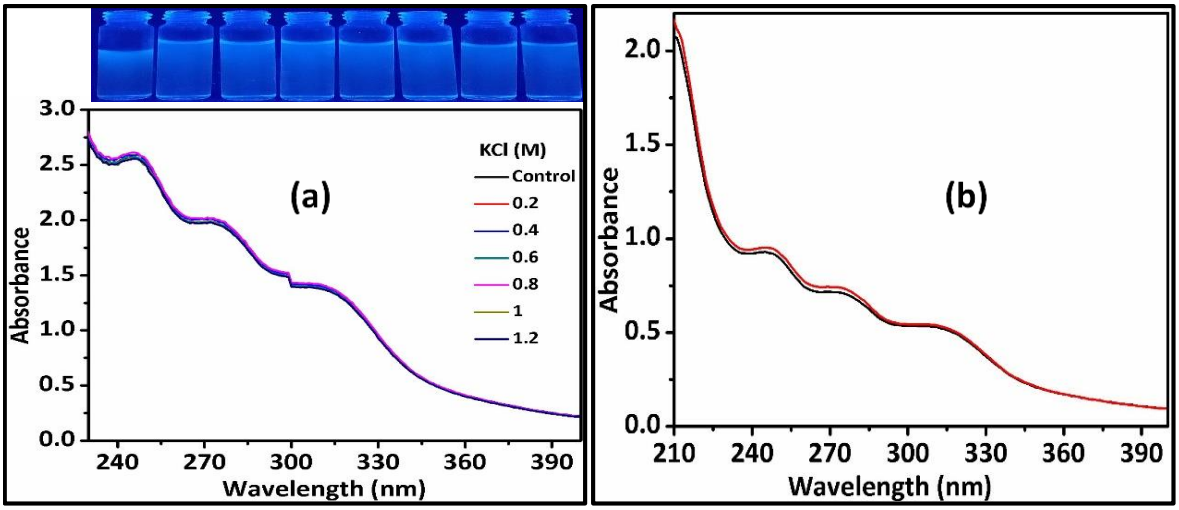

Figure 3.6 (a) Ionic stability of M-CQDs in different concentration of KCl solution with image under UV-Light (λ_{ex}= 365 nm) (b) Photostability of M-CQDs after exposure of normal light for 8 h (red line) with initial absorbance (black line)**.**

3.3.3. Peroxidase-like mimetic activity of M-CQDs

To investigate the catalytic properties of M-CQDs, three set of the experiment were carried out. In the first experiment, the bare TMB solution in NaAc buffer pH 4 showed negligible absorbance at 652 nm, but after in second test the addition of H_2O_2, an appreciable change in absorption at 652 nm was observed. However, in the third experiment, TMB+H_2O_2+M-CQDs in NaAc buffer at pH 4 showed maximum absorption at 652 nm which confirmed the catalytic ability of M-CQDs. This observation was further supported by the change in color from colorless to dark blue as shown in **Figure 3.7**. Hence this result confirmed the peroxidase-like mimic activity of M-CQDs for the oxidation of TMB.

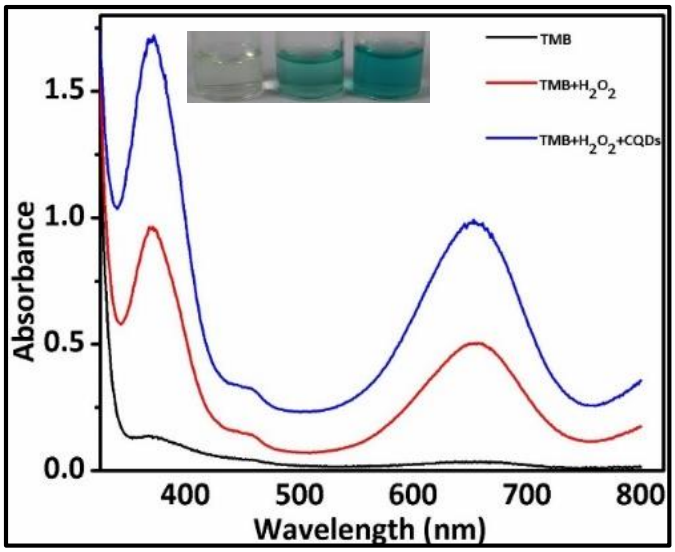

Figure 3.7 UV- visible absorption spectrum of different system in 0.2 M acetate buffer at pH 4, bare TMB (black line), TMB+H_2O_2 (red line) and TMB+H_2O_2+M-CQDs (blue line) with color change **(inset Figure)**.

The peroxidase-like catalytic activity of the M-CQDs was influenced by the change in pH, incubation time, temperature, the concentration of TMB and H_2O_2. Therefore, the catalytic activity was optimized for the above-mentioned parameters. The effect of pH was evaluated at different pH (2 to 6) that showed maximum absorption at pH 4 while the reaction performed at different time interval from 10 to 50 minutes showed maximum absorbance (652 nm) at 40 minutes of incubation time **(Figure 3.8a, c)** which were further confirmed by the appearance of blue color solution (inset). Similarly, the oxidation of TMB was carried out at different temperatures ranging from 10 to 60 ^oC which showed optimum catalytic activity at 40 ^oC of reaction temperature which was confirmed by the development of intense blue color and sharp spectra at 652 nm **(Figure 3.8b).** The effect of substrate concentration on oxidation process was also monitored by varying the concentration of TMB and H_2O_2 which exhibited maximum catalytic activity at 9 mM of TMB and H_2O_2 concentration with an appearance of dark blue color solution **(Figure 3.8d, e)**. Thus the

proposed M-CQDs showed their maximum catalytic activity at pH 4 and 40 minute incubation time, 40 ^{o}C temperature with 9 mM of TMB and H_2O_2 concentration.

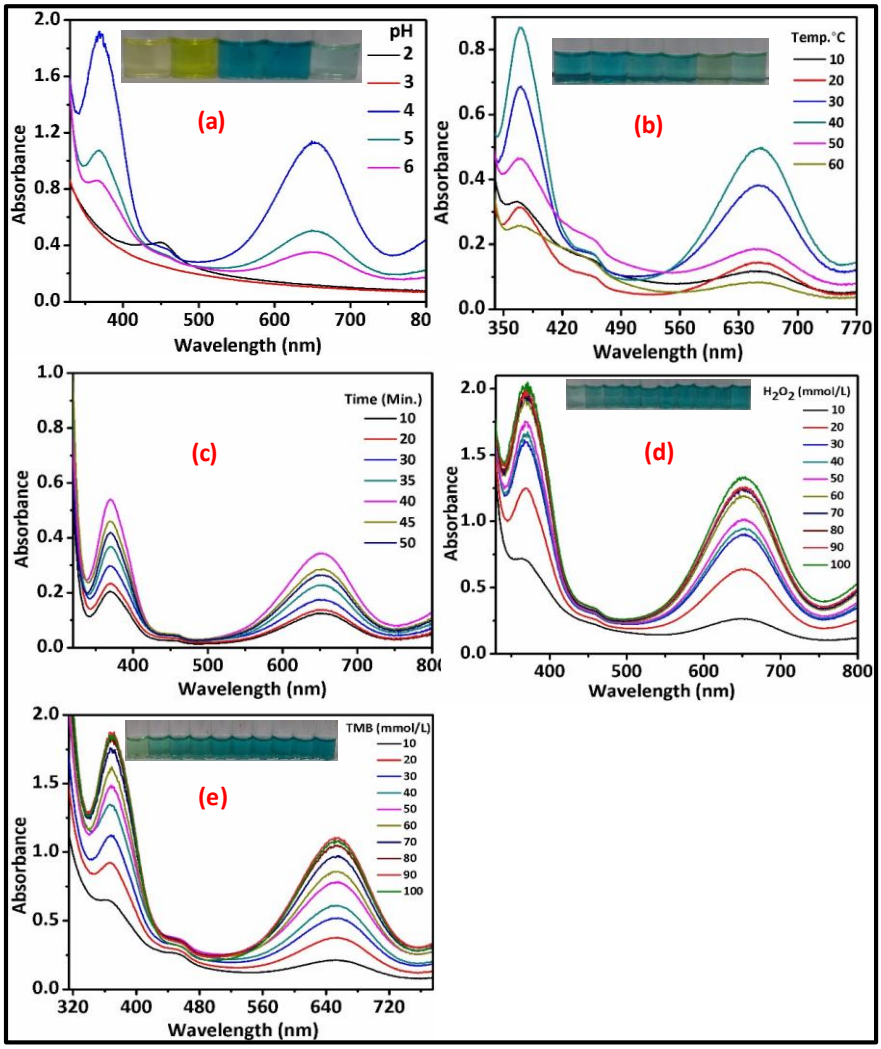

Figure 3.8 Optimization parameter for the oxidation of TMB by M-CQDs at different (a) pH (b) temperature (c) time (d) Concentration of H_2O_2 and (e) Concentration of TMB

3.3.3.1. Steady-state kinetic assay of M-CQDs

The steady-state kinetic assay for the oxidation of TMB by M-CQDs was evaluated by varying the concentration of one substrate and fixing the concentration of another substrate with absorption change at 652 nm with time. The initial rate of reaction was calculated with the change of concentration of TMB with time by utilizing the Beer-

Lambert's law and the molar absorption coefficient 39000 M^{-1} C^{-1} for the oxidized TMB product. The rate of reaction for the oxidation of TMB at various substrates concentration (H_2O_2 and TMB) was calculated by the slope of the absorption variations with reaction time. Initially, the concentration of H_2O_2 was fixed at 1.2 mM and varies the concentration of TMB, and in a same set of reaction TMB was fixed at 1.2 mM, and H_2O_2 varied **(Figure 3.9a, d)**. The Apparent Michaelis-Menton constant (K_m) and maximum velocity (V_{max}) were obtained from using Lineweaver-Burk plot **(Figure 3.9b, e)** and Michaelis-Menton equation 1.

$$\frac{1}{V} = \frac{K_m}{V_{max}} \frac{1}{[S]} + \frac{1}{V_{max}} \qquad 1$$

Where V_{max} = maximum velocity, K_m = Michaelis - Menton constant, V = initial velocity and [S] is the substrate concentration. The catalytic activity of M-CQDs depends upon the K_m value, i.e., lower the K_m value, higher the affinity between enzyme and substrate, hence more catalytic efficiency. The results indicated that the K_m value was lower for TMB as substrate concentration than H_2O_2, which indicated the higher affinity for TMB as compared to H_2O_2. This observation was similar to the natural enzyme horseradish peroxidase (HRP) and reported literature **(Table 3.1).**

Table 3.1 Comparison of the Michaelis–Menten constant (Km and Vmax) of M-CQDs catalyzed oxidation of TMB. Where Km is the Michaelis constant and Vmax is the maximum velocity

Catalyst	**Substrate**	**Km (mM)**	**Vmax**	**Reference**
HRP	TMB H_2O_2	0.434 3.70	10×10^{-8} 8.7×10^{-8}	[Choleva *et al.* (2018)]
Fe_3S_4	TMB H_2O_2	0.160 1.158	1.146×10^{-8} 2.168×10^{-8}	[Ding *et al*. (2016)]
$ZnFe_2O_4$	TMB H_2O_2	0.85 1.66	13.31×10^{-8} 7.74×10^{-8}	[Su *et al*. (2012)
N-GQDs	TMB H_2O_2	0.10 11.19	0.14×10^{-8} 0.38×10^{-8}	[Lin et al. (2015)]
$Fe_3(PO_4)_2(OH)_2$	TMB H_2O_2	0.055 0.47	5.96×10^{-8} 16.88×10^{-8}	[Yang *et al.* (2018)]
M-CQDs	TMB H_2O_2	0.2189 0.4305	0.8819×10^{-6} 0.4611×10^{-5}	**This work**

Moreover, the catalytic activity was further confirmed by double reciprocal plots obtained with the fixed concentration of H_2O_2 over varying the concentration of TMB and vice-versa **(Figure 3.9c, f)**. The slopes of the lines are parallel *viz.* it followed the typical Ping-Pong mechanism which suggested that during the oxidation process, M-CQDs bind with one substrate and released the first product before binding with the second substrate.

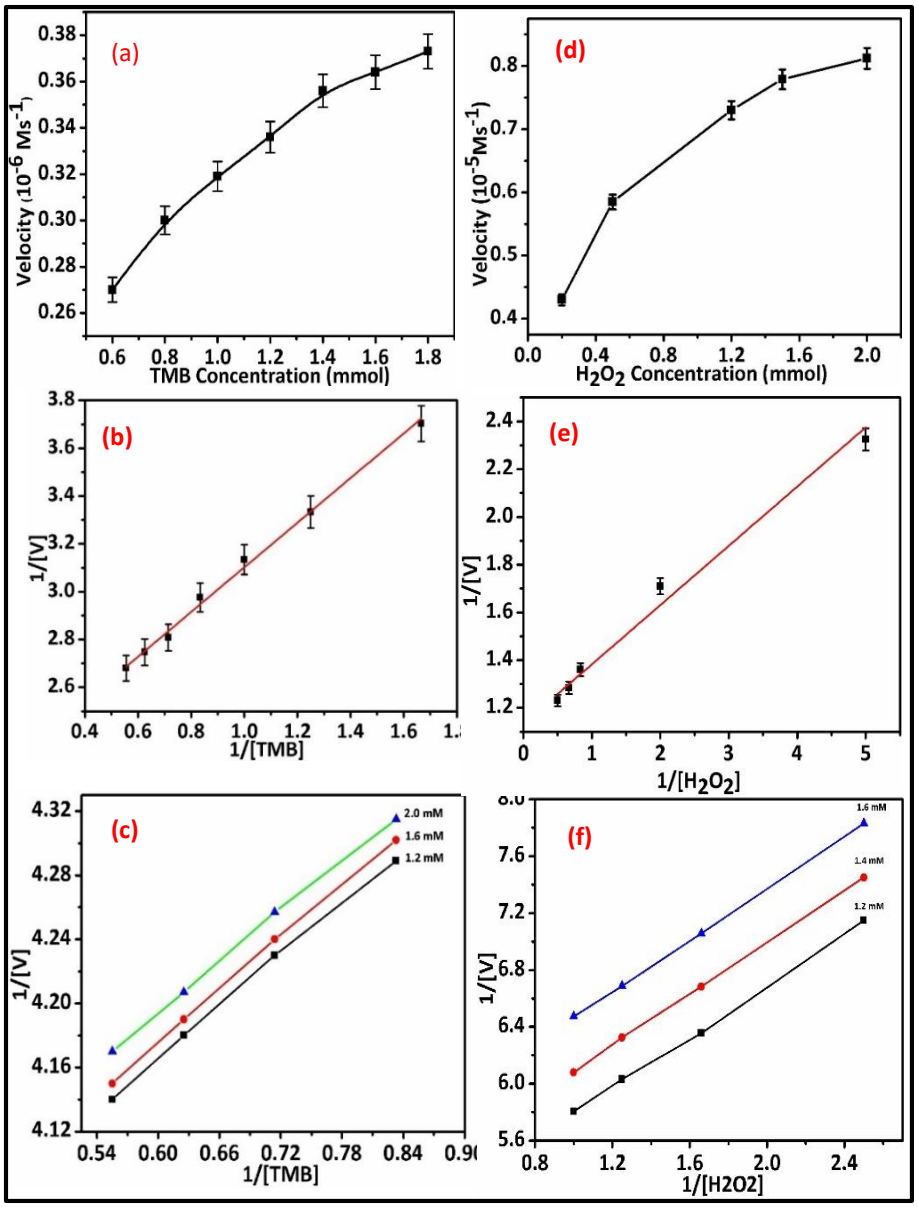

Figure 3.9 Steady-state kinetic assay of the M-CQDs, where the velocity was determined through oxidation of TMB with the corresponding absorption at 652 nm with varying concentrations of (a) TMB and (d) H_2O_2 and the corresponding Lineweaver–Burk plots obtained through fixed the concentration of one with varying the other substrate: (b) Varying the TMB at a fixed H_2O_2 concentration and (e) Varying the H_2O_2 at a fixed TMB concentration, along with the double reciprocal plots: (c) Varying the TMB with keeping H_2O_2 constant and (f) Varying the TMB, H_2O_2 while keeping constant.

3.3.3.2 Possible Mechanism of peroxidase-like mimetic activity

The mechanistic studies of peroxidase-like activity of M-CQDs were investigated by performing the oxidation of TMB in the presence and absence of •OH radical scavengers such as methyl alcohol and isopropyl alcohol. From the **Figure 3.10**, it can be seen that in the presence of methyl alcohol (MA) and isopropyl alcohol (IPA) the absorbance of oxidized TMB at 652 nm decreased as compared to the absence of these scavengers. This observation confirmed that during the oxidation process, •OH radical was formed by the reduction of H_2O_2 that facilitated the electron transfer from •OH radical to TMB, i.e., M-CQDs played a vital role to produced •OH radical. The decrease in catalytic activity in the presence of MA and IPA was due to the consuming •OH radical by these scavenger molecules during oxidation of TMB. This was further confirmed by the color change in the absence and presence of MA and IPA **(inset Figure 3.10a)**.

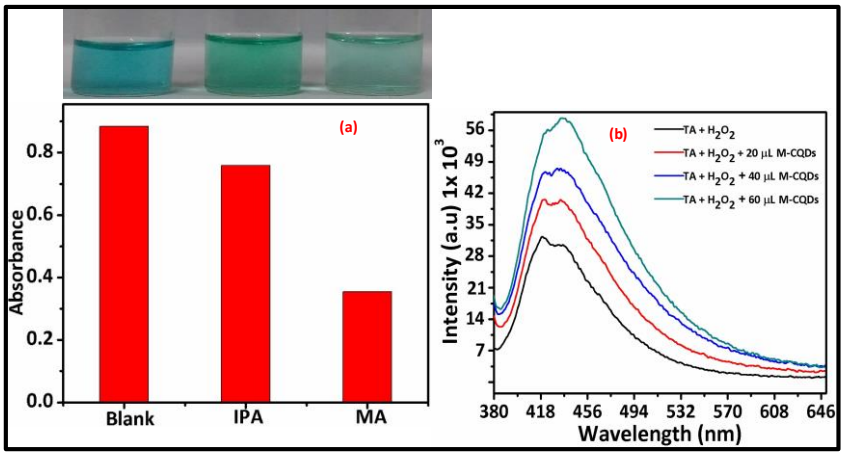

Figure 3.10 (a) Control experiment in the oxidation of TMB in the presence of •OH radical scavenger isopropyl alcohol (IPA) and methyl alcohol (MA). (b) Fluorescence spectra of terephthalic acid in the presence of H_2O_2 and different concentration of M-CQDs indicate the involvement of •OH radical.

To further confirmed the involvement of ˙OH radical fluorescent spectrum of terephthalic acid (TA) in the presence of H_2O_2 and M-CQDs were carried out at λex = 360 nm. From the **Figure 3.10b**, it can be seen that on increasing the M-CQDs (20 to 60 µL) in TA+H_2O_2 solution the emission intensity at 435 nm increases which is the characteristic emission peak of 2-hydroxyterephthalic acid. This observation strongly supports that M-CQDs played a vital role for the formation of ˙OH radical from H_2O_2 resulting the formation of 2-hydroxyterephthalic acid from terephthalic acid. This result confirmed that during oxidation of TMB, M-CQDs generated ˙OH radical from H_2O_2. In addition to this, at the negatively charged M-CQDs, the positively charged TMB accumulated and enhanced the electronic charge on M-CQDs which facilitated the reduction of H_2O_2 to produced ˙OH radical. Hence, the ˙OH radical was undergoing one electron transfer to ease the oxidation of TMB [S.Q *et al.* (2016)]. The overview mechanistic pathway was depicted in **(Scheme 3.2)**.

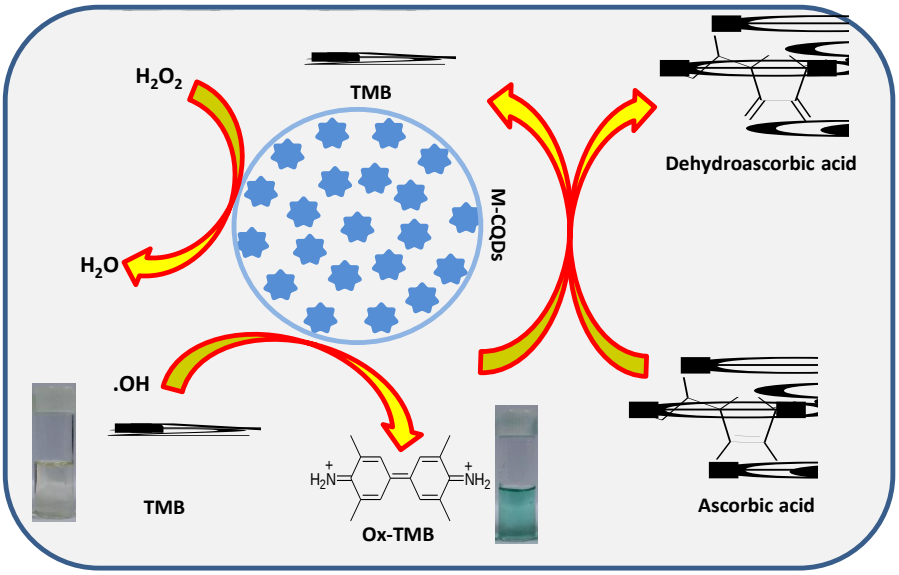

Scheme 3.2 The possible mechanism in favor of peroxidase mimetic activity of M-CQDs and colorimetric detection of H_2O_2 and ascorbic acid.

3.3.3.3 Colorimetric detection of H_2O_2

Hydrogen peroxide is a reactive oxygen species, which played an important role in biological reactions and widely used in many food industries as raw materials [M. Yang *et al*. (2017)]. The excessive use of H_2O_2 as a bactericidal agent caused the deleterious effect on the environment [M. Geiszt *et al.* (2004)]. Therefore, it is an urgent need to design a simple colorimetric method for the detection of H_2O_2. The oxidation of TMB was influenced by the concentration of H_2O_2. Hence, the colorimetric detection of H_2O_2 was demonstrated through oxidation of TMB by adding the H_2O_2 in the range of 0.0 to 7.0 mM concentrations in the reaction mixture (1 mL of 0.2 M NaAc buffer at pH 4 and 50 µL CQDs + 50 µL TMB). As shown in **Figure 3.11a**, the absorbance at 652 nm increased with the proportion of H_2O_2 concentration, and it showed a good linear relation in the concentration range of 0.02 to 0.20 mM with the correlation coefficient (R^2=0.993) **(inset Figure 3.11b)**. The LOD was found to be 0.015 mM with (S/N=3).

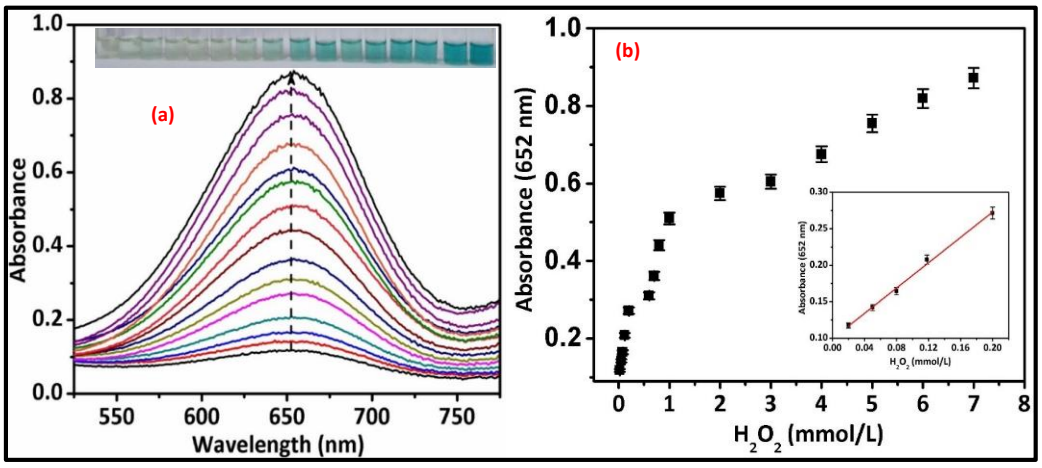

Figure 3.11 (a) Colorimetric detection of H_2O_2 with corresponding color change (b) Change in absorption at 652 nm in the presence of different concentration of H_2O_2 with inset graph shows linear range 0.02-0.2 mM of detection limit 0.015 mM.

The sensing ability of the proposed method was compared to the previously reported HRP as well as other method. From the **Table 3.2**, it can be notice that present method showed lower LOD with appreciable linear range as compared to already reported method. Thus, this observation stated that present detection system is an excellent material for the sensitive detection of H_2O_2.

Table 3.2 Comparison of colorimetric detection of H_2O_2 by M-CQDs with HRP and Carbon based nanoprobe

Method	**probe**	**Linear range (mM)**	**LOD (mM)**	**Ref**
Colorimetric	CuS-MMT	0.03- 0.2	0.024	[Zhang *et al*. (2017)]
Colorimetric	Au@Pt NRs	0.045-1.0	0.045	[Liu *et al*. (2012)]
Colorimetric	Carbon NPs	0.025-1.0	0.02	[Wang *et al.* (2011)]
Colorimetric	CoS	0.05-0.80	0.20	[Yang *et al.* (2016)]
Colorimetric	N-doped Graphene	NA	0.025	[Navadeepthy *et al.* (2017)]
Colorimetric	M-CQDs	0.0**2-0.2**	0.0**15**	**This work**

3.3.3.4. Colorimetric detection of ascorbic Acid

Ascorbic acid (AA) is one of the most important micronutrients, neurochemicals which is essential for the biological reactions and plays a vital role in antioxidants, an enzyme cofactor, balance the oxidative stress of the human body [Y. Jiang *et al*. (2017)]. In addition, AA is generally used as antioxidants in food, beverages, cosmetics and pharmaceuticals industries [A. Meister *et al.* (1992)]. However, the high doses of AA caused many diseases such as scurvy, mental illness, cancers, and cataracts. Therefore, it is

necessary to develop a simple and rapid method for colorimetric detection of AA. We have demonstrated colorimetric detection of AA through peroxidase-like activity of M-CQDs. Therefore, UV-visible titration experiment was carried out upon the addition of different concentration of AA in blue color of ox-TMB. From the **Figure 3.2a**, it was observed that the absorbance of ox-TMB at 652 nm decreases as the concentration of AA increase from 10 to 70 μM. A good linearity was obtained from 10 to 70 μM with the correlation coefficient (R^2=0.9949). The LOD was calculated to be 3.26 μM with the S/N=3 **(Figure 3.2b)**. After comparing the present detection method to the already reported HRP based as well as other carbon based detection system, it was found that the proposed method exhibited lower LOD with excellent linearity range **(Table 3.3)**.

Table 3.3 Comparison of AA detection by M-CQDs with HRP and carbon based different optical sensors.

Methods	**probe**	**Linear range**	**LOD (μM)**	**Reference**
Colorimetric	Reduced Graphene Oxide	5-30	3.6	[Darabdhara *et al*. (2017)]
Colorimetric	MIL-68/MIL-100	30-485	6	[Zhang *et al*. (2014)]
Colorimetric	MIL-53(Fe)	28.6-190.5	15	[L. Ai *et al*. (2013)]
Electrochemistry	CNT	80-136	20	[Wang *et al*. (2002)]
Fluorescence	CdTe QDs	22-240	4.33	[Yang *et al.* (2013)]
Fluorescence	AuNCs	0-120	5	[Hu *et al*. (2014)]
Colorimetric	Cu NPs@C	10-1000	1.41	[Tan *et al.* (2014)]
Colorimetric	M-CQDs	10-75	**3.26**	**This work**

Therefore, M-CQDs mediated ox-TMB based detection system is more reliable, convenient and highly sensitive to real time monitoring of AA in real sample as well as for clinical purpose.

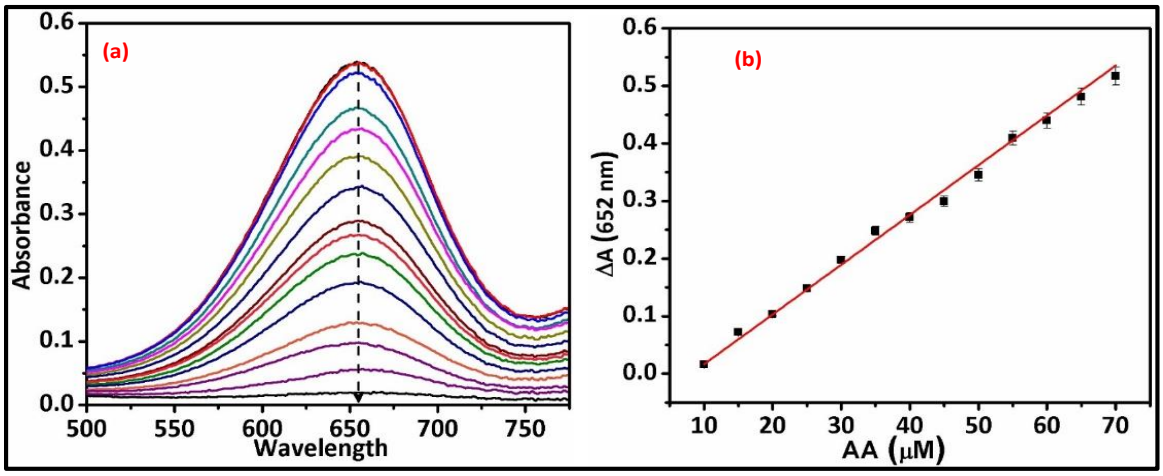

Figure 3.12 (a) ox-TMB based colorimetric detection of ascorbic acid (AA) (b) Change in absorption at 652 nm in the presence of different concentration of AA in the liner range (10 to 70 μM).

Although, the detection of H_2O_2 and AA were based on peroxidase-like activity of M-CQDs via oxidation and reduction of TMB which was totally colorimetric mode. However, fluorescence spectrum of M-CQDs in presence of TMB (M-CQDs+TMB) and H_2O_2 (M-CQDs+TMB+H_2O_2) was quenched due to the ox-TMB. Interestingly, in the presence of AA (M-CQDs+TMB+H_2O_2+AA) the oxidized TMB at the surface of M-CQDs get reduced to native TMB resulting M-CQDs free in the solution and regain its fluorescence property **(Figure 3.13).**

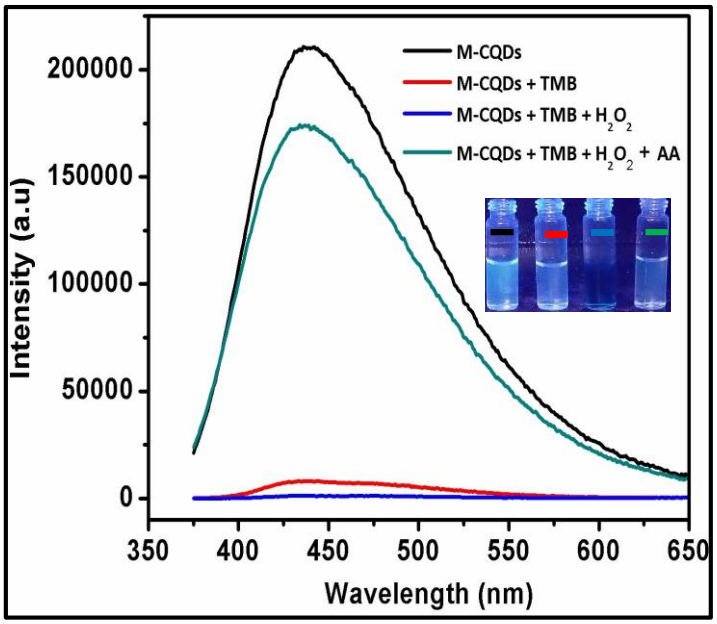

Figure 3.13 Change in fluorescence of M-CQDs in the presence of TMB (red line), TMB+H_2O_2 (blue line) and TMB+H_2O_2+AA (green line) along with colour change (inset photograph).

To evaluate the selectivity of AA detection common reducing agent were introducing in blue color of ox-TMB solution. From the **Figure 3.14**, there was insignificant change in absorbance of ox-TMB at 652 nm in the presence of common reducing agent excluding glutathione (GSH). Although, in the presence of GSH absorbance at 652 nm decrease very less as compare to AA. The drastic decrease in absorption at 652 nm with color change from blue to colorless in the presence of AA indicated the high reduction ability of AA as compare to GSH. This could be due to different structural and functional moieties present in the AA and GSH. Therefore, the proposed method was selective for colorimetric detection of AA.

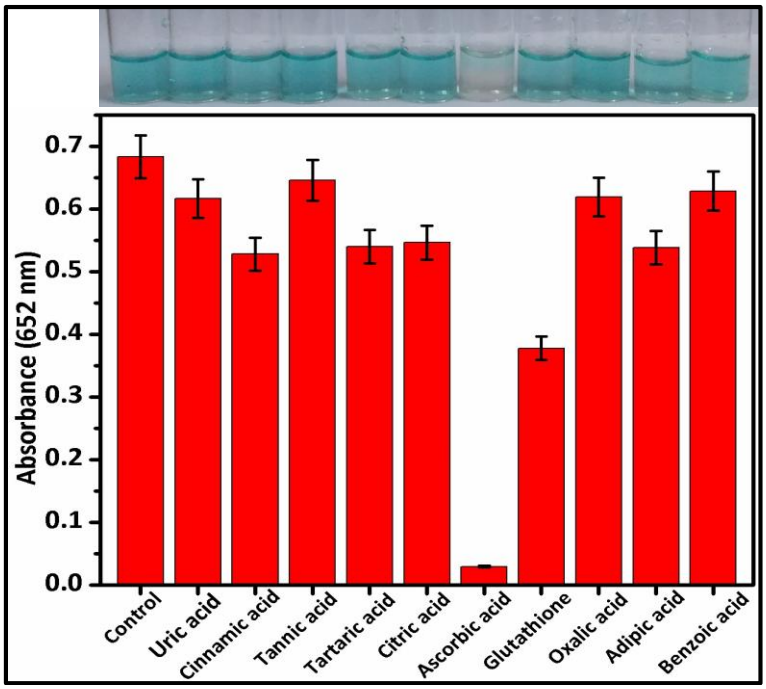

Figure 3.14. Selectivity test of AA detection by ox-TMB in the presence of common reducing agents**.**

3.3.3.5. Colorimetric detection of AA in real fruits Juices

The practical feasibility of AA detection by ox-TMB in the real sample was evaluated in different fruits juices because AA is naturally present in many fruits such as lemon, guava, pineapple, papaya, apple, banana, emblic, mango, orange, and grapes. To estimate the quantifiable analysis of AA in fruit juices, UV-visible titration experiment was performed by addition of fruit juice in the blue color ox-TMB solution. It was noticed that the absorbance at 652 nm gradually decreased with the addition of different fruits juices and the color of the solution changed from blue to colorless. The maximum reduction of ox-TMB occurred in the presence of Emblic juice while the minimum was obtained in pineapple juices confirmed the higher quantity of AA in Emblic juice. Addition to this, the intrinsic color of fruit juices such as (lemon, pineapple, papaya, mango and grapes) does not affect the colorimetric detection of

AA **(Figure 3.15)**. Thus, the proposed sensing system provided an efficient tool for real-time analysis of AA in the biological environment.

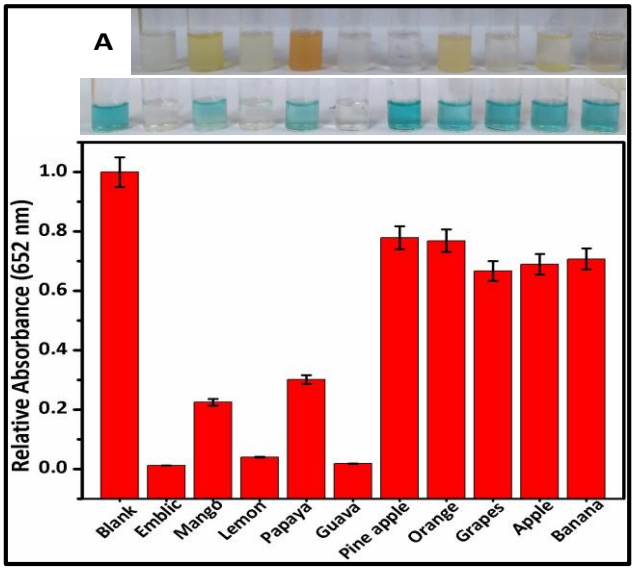

Figure 3.15 Practical feasibility of AA detection by ox-TMB in real sample *viz*. common fruits juice along with photograph of different fruit juice (A).

The anti- interfering ability of the present method was carried out by addition of less AA containing fruits juice (papaya+pineapple+grapes+apple+banana+orange) in the blue color oxidized TMB solution. From the **Figure 3.16**, it was notice that there was no effecting change in absorbance of Ox- TMB at 652 nm in the presence of above mention fruits juice (Mixture 1). However, after addition of high AA containing fruit juice (emblic+mango+lemon+guava) into the mixture 1, the absorbance at 652 nm drastically decrease along with color change blue to colorless. This observation ensured that the proposed method is highly selective for AA detection even in the presence of other reducing agent in fruit juice.

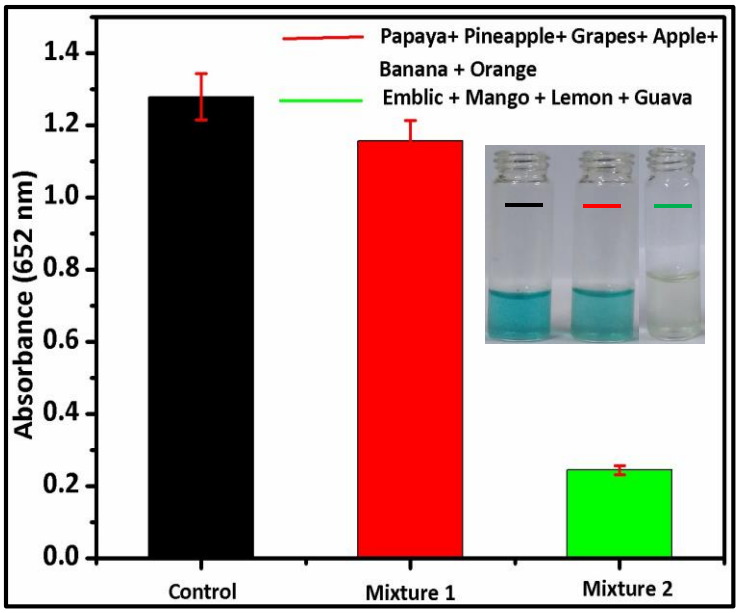

Figure 3.16 Interference test of AA detection in real sample

3.4. Conclusion

In summary, we have synthesized M-CQDs by one step hydrothermal methods from the mustard seeds. The synthesized M-CQDs characterized by various instrumental techniques such as TEM, FT-IR, P-XRD and XPS analysis. It exhibited excellent optical properties and acted as an intrinsic peroxidase-like activity to oxidize the TMB in the presence of H_2O_2 with the production of a blue color solution. The mechanistic studies revealed that M-CQDs helped to generate $^{\bullet}OH$ radical for the oxidation of TMB. The catalytic activity of M-CQDs followed the Michaelis-Menten kinetics behavior and catalytic activity based on Ping-pong type of mechanism. The H_2O_2 dependent oxidation of TMB provided a good platform for the detection of H_2O_2 with the limit of detection 0.015 mM. Interestingly, the blue color ox-TMB was selectively reduced to native TMB by the natural reducing agent AA. Therefore, ox-TMB act as a colorimetric sensor for detection of AA with the LOD at 3.26 µM. This method was employed for analysis of AA in a real sample such fruits juice, which showed

excellent detection according to the quantity of AA in a real sample. Thus, the proposed sensing system is reliable and convenient for clinical diagnosis of AA in a biological environment.